Supporting Information for "Structure-Determining Step in the Hierarchical Assembly of Peptoid Nanosheets"

Babak Sanii, Thomas K. Haxton, Gloria K. Olivier, Andrew Cho, Bastian Barton, Caroline Proulx, Stephen Whitelam, and Ronald N. Zuckermann

Contents

S1. Monolayer compression does not shift the X-ray peak position of a peptoid monolayer.

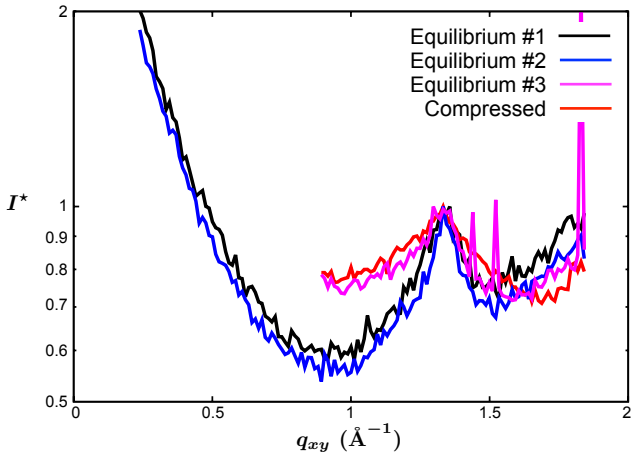

[h]

FIG. S1: Grazing-incidence X-ray scattering spectra of block-28 peptoid monolayers. The spectra labeled Equilibrium #1, 2, and 3 are from independently prepared monolayers at equilibrium with 20 μM block-28 solution. The black spectrum ("Equilibrium #1") is the spectrum used in the main text. The red spectrum ("Compressed") was obtained by compressing the last equilibrium monolayer ("Equilibrium #3," magenta) by 5.8%, then performing grazing-incidence X-ray scattering on a previously unexposed portion of the monolayer while the pressure was actively maintained at its post-compression value.

As shown in Fig. S1, we found that compressing the monolayer did not shift the location of the grazing-incidence X-ray scattering peak. To test the dependence on compression, we first prepared a fresh monolayer at equilibrium with 20 μM block-28 solution (magenta curve in Fig. S1). Note that the peak location of this monolayer agrees with the peak locations of two independently prepared equilibrium monolayers (black and blue curves in Fig. S1), though the peak shape varied somewhat. Next, we compressed the Langmuir trough by 5.8% and performed grazing-incidence X-ray scattering on a previously unexposed portion of the monolayer 2mm away from the original one (red curve in Fig. S1). During the compressed scan the Langmuir trough actively maintained the monolayer's surface pressure within 1% of its post-compression value (34.1 mN/m compared to 28.3 mN/m for the uncompressed monolayer).

If the peptoid monolayer were a homogeneous elastic film, we would expect the 5.8% compression to shift the 4.7 Å (q=1.34 Å^{-1}) peak to 4.4 Å (q=1.41 Å^{-1}). Instead, we found that the compressed peak (red curve in Fig. S1) remained in the same location as the equilibrium peak (magenta curve in Fig. S1) up to the $\approx$ 0.1 Å resolution of the scans. Moreover, the shapes of the equilibrium and compressed X-ray scattering curves nearly superpose. These results are consistent with the computational model that predicts peptoids laterally aggregate at the air-water interface in clusters, leaving bare water in between the clusters. In this model, compression of the monolayer would compress the area between the clusters instead of changing the spacing within the clusters.

S2. Analytic model of monolayer formation

We modeled the temperature- and time-dependent rise in surface pressure with a simple analytic model for the diffusion of dissolved peptoids, activated adsorption onto the interface, and saturation of the monolayer. Our aim was to model the adsorption onto the air-water interface as a function of bulk concentration c_b, temperature T, and time t. We broke the adsorption process into three parts: diffusion of polymers in solution, adsorption onto the interface, and diffusion on the interface. We assumed that adsorption is dominated by isolated, globular peptoids adsorbing from solution, with an adsorption rate controlled by a free energy barrier $\Delta\mathcal{F}(c_\mathrm{b}, T)$. We assumed that the diffusion of peptoids on the interface is only affected by other peptoids already on the interface, *not* by peptoids in the bulk. This assumption allowed us to treat diffusion in the bulk, adsorption to the interface, and diffusion on the interface separately.

Diffusion in the bulk controls the attempt rate for adsorption, and the success rate is controlled both by the free energy barrier and by the saturation of the interface. Our simulation results indicate that peptoids phase separate at low surface concentrations into concentrated and dilute phases. In our analytic model, we approximate this process by assuming that peptoids phase separate into a empty phase and a phase at an equilibrium surface concentration $c_\mathrm{s}^\mathrm{eq}(c_\mathrm{b}, T)$, and we assume that the phase separation is fast compared to the time it takes for peptoids to diffuse, adsorb, and saturate the surface. With these assumptions, we can write the adsorption success rate as

$$k_\mathrm{success} = \exp\left(-\frac{\Delta\mathcal{F}(c_\mathrm{b}, T)}{k_\mathrm{B}T}\right)\left(1 - \frac{c_s(t)}{c_s^\mathrm{eq}(c_\mathrm{b}, T)}\right). \tag{S1}$$

We treat the bulk concentration c_b as constant because each compression cycle only negligibly depletes the bulk concentration at $c_b = 20$ μM.

Since there are few interactions in the dilute bulk, the diffusion onto the surface becomes an effectively one-dimensional problem of polymers diffusing vertically in a column below their "footprint" on the surface. The average spacing between polymers in each column is the characteristic length scale $h(c_\mathrm{b}, T) = c_\mathrm{s}^\mathrm{eq}(c_\mathrm{b}, T)/c_\mathrm{b}$. For the experimental bulk concentration $c_\mathrm{b} = 20$ μM and surface concentration $c_\mathrm{s}^\mathrm{eq} \simeq 0.2$ nm^{-2} (estimated from simulations and/or molecular packing), $h \simeq 20$ μm. Polymers diffuse with a diffusion constant $D(T) = k_\mathrm{B}T/6\pi\eta(T)r_h$, where $k_\mathrm{B} = 1.987\times10^{-3}$ kcal/mol/°K and and the temperature-dependent viscosity of water can be accurately approximated by[1]

$$\eta(T) = (1.002\times10^{-3}\ \text{Pa s})\exp\left(\frac{294.15 - T}{T - 178.15}\left(1.2364 - 1.37\times10^{-3}(294.15 - T) + 5.7\times10^{-6}(294.15 - T)^2\right)\right). \tag{S2}$$

Assuming a spherical globular polymer, the hydrodynamic radius relates to the radius of gyration *via* $r_h = \sqrt{5/3}r_g$. We use $r_g = 0.89$ nm for block-28 peptoids from the Guinier analysis of the simulated solution X-ray scattering.

The characteristic time scale for diffusion is $h^2/D \simeq 2$ sec, much faster than the 100-1000 sec experimental adsorption time scale observed in Fig. S2. This means that diffusion in the bulk is fast relative to the success rate, and we can assume that the bulk maintains a uniform concentration all the way up to the interface. The attempt rate per column is therefore given by $D(T)/h^2$, and the in the case of 100% success the surface concentration would increase at a rate $Dc_\mathrm{s}^\mathrm{eq}/h^2 = Dc_\mathrm{b}^2/c_\mathrm{s}^\mathrm{eq}$. Combining with Eq. S1 we get an equation for the increase in surface concentration,

$$\frac{dc_\mathrm{s}(t)}{dt} = \frac{Dc_\mathrm{b}^2}{c_\mathrm{s}^\mathrm{eq}}\exp\left(-\frac{\Delta\mathcal{F}}{k_\mathrm{B}T}\right)\left(1 - \frac{c_s(t)}{c_s^\mathrm{eq}}\right). \tag{S3}$$

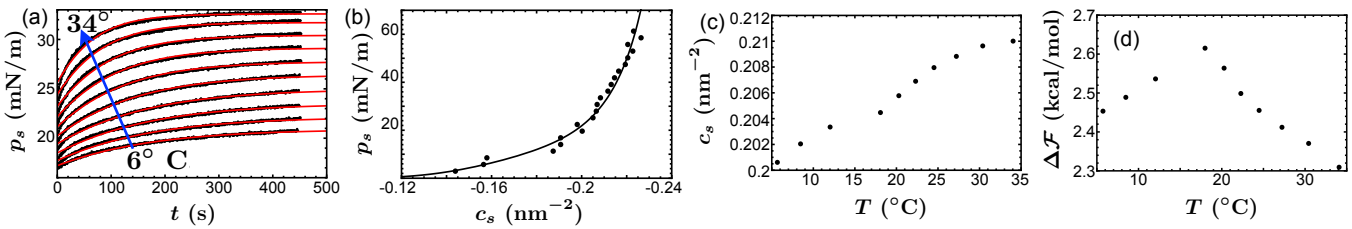

FIG. S2: (a) Time-dependent surface adsorption shows faster adsorption at higher temperatures. Our analytic model (smooth red curves in (a)) reproduces the experimental adsorption curves. (b) Simulated equation of state (points) and polynomial fit (curve) used in the analytic model. (c-d) Temperature dependence of the model fit parameters shows that the equilibrium surface concentration increases with temperature while the free energy barrier for adsorption decreases. Panels (a), (c), and (d) are reproduced from Fig. 6 of the main text.

The solution to Eq. S3 is

$$c_s(c_\mathrm{b},T;t) = c_\mathrm{s}^\mathrm{eq}(c_\mathrm{b},T) + (c_s(0) - c_\mathrm{s}^\mathrm{eq}(c_\mathrm{b},T)) \times \exp\left(-D(T)\left(\frac{c_\mathrm{b}}{c_\mathrm{s}^\mathrm{eq}(c_\mathrm{b},T)}\right)^2 \exp\left(-\frac{\Delta\mathcal{F}(c_\mathrm{b},T)}{k_\mathrm{B}T}\right)t\right). \tag{S4}$$

We converted the time-dependent surface concentration $c_\mathrm{s}(t)$ to a time-dependent surface pressure $p_\mathrm{s}(t)$ using the simulated equation of state $p_\mathrm{sim}(c_\mathrm{sim}, T_\mathrm{room})$. This assumes that the surface pressure relaxes fast compared to the adsorption process; i.e., the monolayer stays close to equilibrium. As shown in Fig. S2 (b), we first applied a polynomial fit to the equation of state to smooth the data. Since we only calculated the simulated equation of state for a coarse-grained model parameterized at room temperature, we accounted for the lowest order effect of temperature by renormalizing the pressure by the temperature. With this renormalization, our conversion from surface concentration to surface pressure is

$$p_\mathrm{s}(c_\mathrm{b},T;t) = \frac{T}{T_\mathrm{room}} p_\mathrm{s}^\mathrm{sim}(c_\mathrm{s}(c_\mathrm{b},T;t), T_\mathrm{room}). \tag{S5}$$

Combining Eqs. S4 and S5, we found an expression for the time-dependent surface pressure $p_\mathrm{s}(c_\mathrm{b},T;t)$ that depends on three free parameters, $c_\mathrm{s}^\mathrm{eq}(c_\mathrm{b},T)$, $\Delta\mathcal{F}(c_\mathrm{b},T)$, and $c_\mathrm{s}(0)$. The first two characterize the equilibrium surface density and the free energy barrier for adsorption, respectively. They are state-dependent; both the equilibrium surface density and the free energy barrier may depend on the bulk concentration and temperature. The last parameter is the initial condition that depends on how far the monolayer was decompressed before adsorption. Figure S2 (c) and (d) show the temperature dependence of $c_\mathrm{s}^\mathrm{eq}(c_\mathrm{b},T)$ and $\Delta\mathcal{F}(c_\mathrm{b},T)$ at $c_\mathrm{b} = 20\ \mu$M.

S3. Dependence of nanosheet yield on temperature and wait-time

	20C	40C	60C
30s wait time	0.28	0.78	**1.0**
100s wait time	0.08	0.36	0.89
420s wait time	–	0.30	0.29

TABLE SI: Dependence of relative nanosheet yield on temperature and wait-time.

Table SI shows the dependence of nanosheet yield on temperature and wait-time. Relative peptoid nanosheet production was measured by fluorescence (see main text methods section) at three temperatures (20, 40, and 60C) and three wait-times (30s, 100s, 420s). Relative production is in terms of nanosheets per hour, including the time spent waiting for the monolayer to regenerate. Nanosheet production with a 420s wait time and 20C was too low to be measured by this technique. The relative production rates are scaled to the highest producing conditions tested: 30s wait-time and 60C.

S4. Resilience to electron beam damage

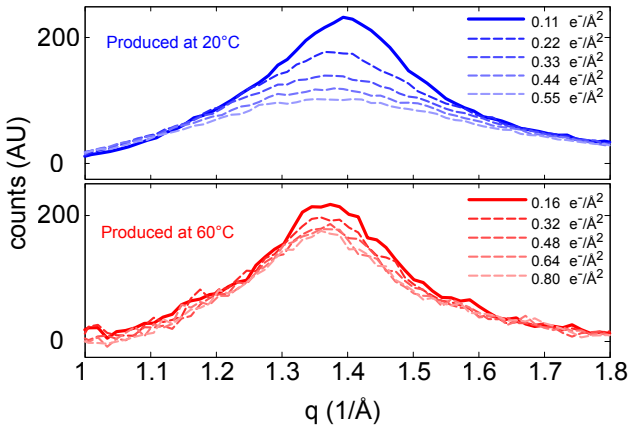

FIG. S3: Radially averaged electron diffraction spectra of block-28 peptoid nanosheets produced at room temperature (above, blue) and at 60C (below, red), at increasing cumulative exposure to 200kV electrons.

Consecutive electron diffraction measurements can be used to determine the resiliency of the structure of a material to electron beam damage.[2] Diffraction spots or rings fade with cumulative exposure, indicating increasing disorder. Here we exposed peptoid nanosheets to consecutive electron diffraction measurements and observed the relative resiliency of peptoid nanosheets produced at greater temperatures.

Two batches of peptoid nanosheets were produced with the vial-rotation method described in the main text, one batch at 20C and another at 60C. Nanosheets were cooled to room temperature and deposited onto grids in 1-2 μL droplets. The excess solution was subsequently wicked away with filter paper after 1-2 minutes. Free-standing nanosheets were identified by low-magnification TEM imaging on a Libra 200MC at the National Center for Electron Microscopy, and a diffraction pattern was recorded at 200 keV electron energy and a camera length of 750 mm, using zero-loss energy filtering (slit size 5eV) on an area of approximately $4\mu m^2$. The diffraction ring visible in the patterns suggest an isotropic ordering in both samples. The 60C nanosheet had a diffraction peak corresponding to 4.6, the 20C had one corresponding to 4.5.

A series of exposures showed a significant cumulative dose-dependent decay (see Fig. S3) in the radially averaged diffraction patterns of the nanosheet produced at 20C. The nanosheet produced at 60C demonstrated greater resiliency to electron beam damage.

S5. Surface pressure vs concentration

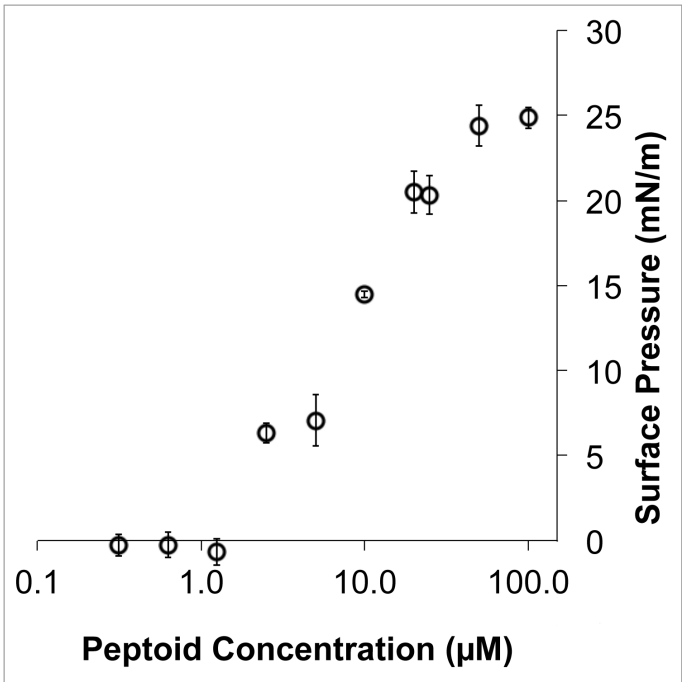

FIG. S4: Surface tension vs. concentration of Block-28 peptoids was measured by capillary rise using a custom-built device. The device consists of a fixed horizontal camera, lens, and light source and a vertical translation stage that holds the sample and the capillary. Glass capillaries of 0.58mm inner diameters were ambient-air plasma-etched (3 min, Harrick, Ithaca, NY), and one end was dipped into freshly mixed solution (within 1 min of mixing). The base liquid level was determined by aligning it to a mark in the middle of the cameras field of view. The capillary rise was measured by the amount of vertical translation necessary to place the bottom of the meniscus inside the capillary on the same mark in the cameras field of view. Capillary rise measurements were corrected for the meniscus by adding the inner radius/3. The surface tension was calculated with the formula $\gamma = \rho grh/(2cos\theta)$,[3] where is surface tension, ρ is the density of the liquid, g is the acceleration due to gravity, r is the inner radius of the capillary, h is the measured height of the capillary action, and θ is the contact angle of the solution on glass (measured to be $< 5°$; $cos(\theta)$ is approximated as 1). For the surface tension measurements peptoid was dissolved in water with 100 mM NaCl, 10 mM AMPD (pH 9), 0.67% DMSO (v/v).

REFERENCES

1. Kestin, J.; Sokolov, M.; Wakeham, W. A. Viscosity of Liquid Water in Range -8 Degrees C to 150 Degrees C. *J. Phys. Chem. Ref. Data* **1978**, *7*, 941.

2. Grubb. D. T. Review Radiation-Damage and Electron-Microscopy of Organic Polymers. *J. Mater. Sci.* **1974**, *9*, 1715.

3. de Gennes, P.-G. Wetting–Statics and Dynamics. *Rev. Mod. Phys.* **1985**, *57*, 827.